Cooperative scattering and radiation pressure force in dense atomic clouds

Romain Bachelard, Nicola Piovella, Philippe W. Courteille

Cooperative scattering and radiation pressure force in dense atomic clouds

R. Bachelard[a], N. Piovella[b], and Ph. W. Courteille[c]
[a] *University of Nova Gorica, School of Applied Sciences, Vipavska 11c SI-5270 Ajdovcina, Slovenija*
[b] *Dipartimento di Fisica, Università Degli Studi di Milano, Via Celoria 16, I-20133 Milano, Italy*
[c] *Instituto de Física de São Carlos, Universidade de São Paulo, 13560-970 São Carlos, SP, Brazil.*
(Dated: March 30, 2011)

We consider the collective scattering by a cloud of N two-level atoms driven by an uniform radiation field. Dense atomic clouds can be described by a continuous density and the problem reduces to deriving the spectrum of the atom-atom coupling operator. For clouds much larger than the optical wavelength, the spectrum is treated as a continuum, and analytical expressions for several macroscopic quantities, such as scattered radiation intensity and radiation pressure force, are derived. The analytical results are then compared to the exact N-body solution and with those obtained assuming a symmetric timed Dicke state. In contrast with the symmetric timed Dicke state, our calculations takes account of the back action of the atoms on the driving field leading to phase shifts due to the finite refraction of the cloud.

I. INTRODUCTION

Cooperative scattering by many atoms has been studied extensively in the past, both classically and quantum-mechanically. Classically, scattering at extended objects is described as Mie scattering, showing resonances induced by the boundary conditions that the target imposes to the incident light field [1]. Quantum-mechanically, Dicke [2] has shown that, when two-level atoms are confined inside a volume much smaller than a radiation wavelength, the emission can be superradiant or subradiant. How the classical and quantum pictures are linked has been demonstrated at the example of a sample of weakly excited atoms [3, 4]. More precisely, when a single atom out of N is excited, the Dicke symmetric state of maximum cooperation radiates superradiantly, i.e. at a decay rate proportional to N. Cooperative effects related to the superradiant and directional emission by an extended ensemble of atoms in a phased (or 'timed') symmetric Dicke state have been observed in the radiation pressure force acting on a large cloud of atoms driven by a resonant radiation field. Depending on the detuning of the incident radiation frequency from atomic resonance, the radiation pressure force may be either drastically reduced due to both increased forward scattering and a reduced scattering cross section [5, 6], or even enhanced if the cooperative Mie scattering dominates over superradiance [7].

In this paper we revisit the scattering by N atoms driven by a constant uniform radiation field and emitting radiation into free space. Our description assumes several approximations: 1) weak excitation of the atomic ensemble (one atom out of N is excited); 2) Markov or 'rapid transit' approximation [3] (photon time of flight through the cloud much shorter than atomic decay time); 3) atoms frozen (zero temperature) and motionless; 4) neglected dipole-dipole interactions and collisions; 5) no resonant interactions, as e.g. no resonance fluorescence, Van der Waals interactions etc. Approximation 3) excludes several cooperative effects related to atomic recoil motion (e.g. collective atom recoil lasing [8, 9] or matter wave superradiance [10, 11]), and thus neglects stimulated scattering processes along preferential directions, as for instance end-fire modes in Bose-Einstein condensates [12] or optical cavity modes [13]. Neglecting atomic interactions (approximation 4)) is justified assuming atomic ensemble sizes much larger than an optical wavelength. The yet interesting opposite regime (atoms closer than an optical wavelength) requires the solution of the atomic equations with an exponential interaction kernel (see Eq.(3)) and will be referred to a future publication.

Solving the eigenvalue problem in the continuous density approximation for a spherical Gaussian distribution, we find the stationary solution and relevant macroscopic quantities, such as medium polarization, scattered radiation intensity and radiation pressure force. For large sample size, a continuous spectrum approximation allows to obtain explicit analytical expressions for such quantities, expressed as a function of experimentally controllable parameters such as frequency and power of the driving field, optical thickness and size of the atomic sample. In Sec.II the scattering problem is expressed in terms of multi-particle coupled differential equations. In Sec.III the continuous density approximation is introduced and the solution for the atomic field is found in terms of the discrete eigenvalues of the interaction operator. Then, several macroscopic quantities are calculated in Sec.IV. A continuous spectrum approximation for large atomic clouds performed in Sec.V appears to be particularly suitable to evaluate macroscopic quantities for arbitrarily large value of the atomic density. Sec. VI revises the radiation pressure force obtained assuming a symmetric timed Dicke atomic state[5]. Comparing this state to the exact solution, we will find that phase shifts induced by the atomic cloud's refractive index are at the origin of important corrections for the expectation values of macroscopic quantities. Finally, numerical results and conclusions are presented in Sec.VII.

II. COOPERATIVE SCATTERING PROBLEM

A system of two-level (g and e) atoms with resonant frequency ω_a and position $\mathbf{r}_j$, driven by an uniform laser beam with electric field amplitude E_0, frequency ω_0 and wave vector $\mathbf{k}_0 = (\omega_0/c)\hat{\mathbf{e}}_z$, is described by the interaction Hamiltonian:

$$\begin{aligned} H &= \frac{\hbar\Omega_0}{2}\sum_{j=1}^{N}\left[\hat{\sigma}_j e^{i(\Delta_0 t-\mathbf{k}_0\cdot\mathbf{r}_j)}+\text{h.c.}\right] \\ &+ \hbar\sum_{j=1}^{N}\sum_{\mathbf{k}} g_k\left(\hat{\sigma}_j e^{-i\omega_a t}+\hat{\sigma}_j^{\dagger}e^{i\omega_a t}\right)\left[\hat{a}_{\mathbf{k}}^{\dagger}e^{i(\omega_k t-\mathbf{k}\cdot\mathbf{r}_j)}+\hat{a}_{\mathbf{k}}e^{-i(\omega_k t-\mathbf{k}\cdot\mathbf{r}_j)}\right] \end{aligned} \tag{1}$$

where $\Omega_0 = dE_0/\hbar$ is the Rabi frequency of the incident laser field, $\hat{\sigma}_j$ is the lowering operator for atom j, $\hat{a}_{\mathbf{k}}$ is the photon annihilation operator and $g_k = (d^2\omega_k/2\hbar\epsilon_0 V_{ph})^{1/2}$ is the atom-photon coupling constant, where d is the electric-dipole transition matrix element and V_{ph} is the photon volume. A special case is when a single photon is present in the mode $\mathbf{k}$, as was extensively investigated in Refs.[14–16]. The total system (atoms+photons) is assumed to be in a state of the form [4]:

$$\begin{aligned} |\Psi\rangle &= \alpha(t)|g_1\dots g_N\rangle|0\rangle_{\mathbf{k}} + e^{-i\Delta_0 t}\sum_{j=1}^{N}\beta_j(t)|g_1\dots e_j\dots g_N\rangle|0\rangle_{\mathbf{k}} + \sum_{\mathbf{k}}\gamma_{\mathbf{k}}(t)|g_1\dots g_N\rangle|1\rangle_{\mathbf{k}} \\ &+ \sum_{m,n=1}^{N}\epsilon_{m<n,\mathbf{k}}(t)|g_1\dots e_m\dots e_n\dots g_N\rangle|1\rangle_{\mathbf{k}}, \end{aligned} \tag{2}$$

where $\Delta_0 = \omega_0 - \omega_a$. The first term corresponds to the initial ground state without photons, the sum in the second term are the states where a single atom has been excited by the classical field. The third term corresponds to the atom returned to the ground state having emitted a photon in the mode $\mathbf{k}$, whereas the last one corresponds to the presence of two excited atoms and one virtual photon with 'negative' energy. Its presence is due to the not Rotating Wave Approximation (RWA) terms in the Hamiltonian (1). In the linear regime (i.e. $\alpha \approx 1$) and in the Markov approximation (valid if the decay time is larger than the photon time-of-flight through the atomic cloud), the problem reduces to the following differential equation [19],

$$\dot{\beta}_j = \left(i\Delta_0 - \frac{\Gamma}{2}\right)\beta_j - i\frac{\Omega_0}{2}e^{i\mathbf{k}_0\cdot\mathbf{r}_j} + i\frac{\Gamma}{2}\sum_{m\neq j}\frac{\exp(ik_0|\mathbf{r}_j-\mathbf{r}_m|)}{k_0|\mathbf{r}_j-\mathbf{r}_m|}\beta_m, \tag{3}$$

where $\Gamma = V_{ph}g_k^2k_0^2/\pi c$ is the single-atom *spontaneous* decay rate. The last term in Eq.(3) has a real component, $-(\Gamma/2)\sum_{m\neq j}[\sin(\rho_{jm})/\rho_{jm}]\beta_m$ (where $\rho_{jm} = k_0|\mathbf{r}_j - \mathbf{r}_m|$), describing the *collective* atomic decay, and an imaginary component, $i(\Gamma/2)\sum_{m\neq j}[\cos(\rho_{jm})/\rho_{jm}]\beta_m$, describing the collective Lamb shift due to short range interaction between atoms, induced by the electromagnetic field [19–21]. The latter becomes significant when the number of atoms in a cubic optical wavelength, $n\lambda^3$, is smaller than unity, in which case the contribution from the virtual processes described by the not-RWA terms in the Hamiltonian becomes relevant. However, it was shown that for sufficiently large atomic cloud the collective phase shift arising from this term can be disregarded [22]. In this paper we will consider only the large cloud case, i.e. with size $\sigma_R \gg \lambda$, considering only the real part of the kernel in Eq.(3) and neglecting the collecting phase shift. Hence, our scattering problem reduces to solve the equations

$$\dot{\beta}_j = \left(i\Delta_0 - \frac{\Gamma}{2}\right)\beta_j - i\frac{\Omega_0}{2}e^{i\mathbf{k}_0\cdot\mathbf{r}_j} - \frac{\Gamma}{2}\sum_{m\neq j}\frac{\sin(k_0|\mathbf{r}_j-\mathbf{r}_m|)}{k_0|\mathbf{r}_j-\mathbf{r}_m|}\beta_m. \tag{4}$$

with initial condition $\beta_j(0) = 0$, for $j = 1,\dots,N$. Notice that Eq.(3) deduced in the quantum mechanical description may be also obtained classically when the two-level atoms are treated as weakly excited classical harmonic oscillators [3, 4]. For this reason the solution of Eq.(3) (or of the approximated version (4)) has a wider interest for the general problem of collective radiation scattering.

III. DENSE CLOUDS

When the cloud is dense enough, typically when the number of particles in a volume λ^3 is large, the stochastic fluctuations induced by the random positions of the atoms are neglected, the particles are modelled by a continuous

density $n(\mathbf{r})$ and their probability to be excited by a field $\beta(\mathbf{r},t)$. The high-density limit of Eq.(4) then reads

$$\frac{\partial}{\partial t}\beta(\mathbf{r},t) = \left(i\Delta_0 - \frac{\Gamma}{2}\right)\beta(\mathbf{r},t) - i\frac{\Omega_0}{2}e^{i\mathbf{k}_0\cdot\mathbf{r}} - \frac{\Gamma}{2}\int \mathrm{d}\mathbf{r}' n(\mathbf{r}')\frac{\sin(k_0|\mathbf{r}-\mathbf{r}'|)}{k_0|\mathbf{r}-\mathbf{r}'|}\beta(\mathbf{r}',t). \tag{5}$$

In what follows we will consider only spherically symmetric distributions $n(r)$. Because of the linearity of Eq.(5), it is convenient to introduce an eigenbasis of the coupling operator. The functions $j_n(r)Y_{nm}(\theta,\phi)$, with j_ns the spherical Bessel functions and $Y_{nm}(\theta,\phi)$s the spherical harmonics, appear as a natural choice considering the following identity

$$\frac{\sin(k_0|\mathbf{r}-\mathbf{r}'|)}{k_0|\mathbf{r}-\mathbf{r}'|} = 4\pi\sum_{n=0}^{\infty}\sum_{m=-n}^{n} j_n(k_0 r)Y^*_{nm}(\theta,\phi)Y_{nm}(\theta',\phi')j_n(k_0 r'). \tag{6}$$

In particular, the choice of the spherical harmonics guarantees the orthogonality of the basis, since

$$\int_0^{2\pi}\mathrm{d}\phi\int_0^{\pi}\mathrm{d}\theta\sin\theta Y^*_{nm}(\theta,\phi)Y_{n'm'}(\theta,\phi) = \delta_{nn'}\delta_{mm'}. \tag{7}$$

Therefore, assuming the following decomposition for the field,

$$\beta(\mathbf{r},t) = \sum_{n=0}^{\infty}\sum_{m=-n}^{n}\alpha_{nm}(t)j_n(k_0 r)Y_{nm}(\theta,\phi), \tag{8}$$

the projection of Eq.(5) along the eigenmodes leads to

$$\left[\dot{\alpha}_{nm} - i\Delta_0\alpha_{nm} + \frac{\Gamma}{2}(1+\lambda_n)\alpha_{n,m}\right]j_n(k_0 r) = -\frac{i}{2}\Omega_{nm}, \tag{9}$$

where λ_n are the eigenmodes associated to modes n

$$\lambda_n = 4\pi\int_0^{\infty} r^2 n(r)j_n^2(k_0 r)\mathrm{d}r \tag{10}$$

whereas Ω_{nm} corresponds to the projection of the incident wave on mode (n,m)

$$\Omega_{nm} = \Omega_0\int_0^{2\pi}\mathrm{d}\phi\int_0^{\pi}d\theta\sin\theta\, Y^*_{nm}(\theta,\phi)\, e^{ik_0 r\cos\theta} = 2\Omega_0\delta_{m0}\sqrt{\pi(2n+1)}i^n j_n(k_0 r). \tag{11}$$

Assuming the cloud is initially unexcited, i.e. $\alpha_{mn}(0)=0$, only spherically symmetric components with $m=0$ will grow so that, defining $\alpha_n(t)\equiv\alpha_{n0}(t)$, Eq.(9) reduces to

$$\dot{\alpha}_n - \left[i\Delta_0 - \frac{\Gamma}{2}(1+\lambda_n)\right]\alpha_n = -i^{n+1}\sqrt{\pi(2n+1)}\Omega_0 \tag{12}$$

Eq.(12) straightforwardly integrates and, inserted in Eq.(8), leads to the following expression for the excitation field

$$\beta(r,\theta,t) \;=\; \frac{\Omega_0}{\Gamma}\sum_{n=0}^{\infty}\frac{i^n(2n+1)j_n(k_0 r)P_n(\cos\theta)}{2\delta + i(1+\lambda_n)}\left[1 - e^{i\Delta_0 t}e^{-(\Gamma/2)(1+\lambda_n)t}\right], \tag{13}$$

where the scaled detuning $\delta = \Delta_0/\Gamma$ was introduced. Hence, each mode n relaxes toward the steady-state with a characteristic time $\tau_n = 1/\Gamma(1+\lambda_n)$: the first modes relax very quickly since λ_n is proportional to N, yet for the highest modes, $\tau_n \sim \Gamma^{-1}$, even if their macroscopic contribution is usually small. Eventually, for times much longer than the single-atom decay time Γ^{-1}, the field tends toward a stationary state fully characterized by the spectrum

$$\beta_s(r,\theta) \;=\; \frac{\Omega_0}{\Gamma}\sum_{n=0}^{\infty}\frac{i^n(2n+1)}{2\delta + i(1+\lambda_n)}j_n(k_0 r)P_n(\cos\theta). \tag{14}$$

Notice that the set of eigenvalues (10) is complete since from the identity $\sum_{n\geq 0}(2n+1)j_n^2(z)=1$, it follows that

$$\sum_{n=0}^{\infty}(2n+1)\lambda_n = 4\pi\int_0^{\infty} r^2 n(r)\mathrm{d}r = N, \tag{15}$$

which corresponds to the trace of the coupling operator.

IV. MACROSCOPIC QUANTITIES

The description of the field $\beta_s(r,\theta)$ in terms of spectrum also provides expressions for any macroscopic quantities, the most relevant of which are calculated here below. These formulae will be specialized to Gaussian clouds in the subsequent section.

A. Average amplitude and probability of excitation

The average 'phased' probability of the timed Dicke state [19] and the excitation probability are respectively

$$\langle \beta_s e^{-i\mathbf{k}_0\cdot\mathbf{r}}\rangle = \frac{2\pi}{N}\int_0^\pi \mathrm{d}\theta \sin\theta \int_0^\infty \mathrm{d}r r^2 n(r)\beta_s(r,\theta)e^{-ik_0 r\cos\theta} \tag{16}$$

$$\langle |\beta_s|^2\rangle = \frac{2\pi}{N}\int_0^\pi \mathrm{d}\theta \sin\theta \int_0^\infty \mathrm{d}r r^2 n(r)|\beta_s(r,\theta)|^2. \tag{17}$$

Inserting Eq.(14) and using the identities

$$\int_{-1}^{1}\mathrm{d}x P_n(x)e^{i\alpha x} = 2i^n j_n(\alpha) \quad , \quad \int_{-1}^{1} dx\, P_m(x)P_n(x) = \frac{2}{2n+1}\delta_{mn}, \tag{18}$$

we obtain

$$\langle \beta_s e^{-i\mathbf{k}_0\cdot\mathbf{r}}\rangle = \frac{\Omega_0}{\Gamma N}\sum_{n=0}^{\infty}\frac{(2n+1)\lambda_n}{2\delta + i(1+\lambda_n)} \tag{19}$$

$$\langle |\beta_s|^2\rangle = \frac{\Omega_0^2}{\Gamma^2 N}\sum_{n=0}^{\infty}\frac{(2n+1)\lambda_n}{4\delta^2 + (1+\lambda_n)^2}. \tag{20}$$

B. Scattered field

A measure of the scattered radiation in the Markov approximation is provided by the scalar field operator

$$\hat{E}_S = \frac{dk_0^2}{4\pi\epsilon_0 r}e^{ik_0(r-ct)+i\Delta_0 t}\sum_{j=1}^{N}\hat{\sigma}_j e^{-i\mathbf{k}\cdot\mathbf{r}_j} \tag{21}$$

propagating along the direction of the mode $\mathbf{k} = k_0(\sin\theta\cos\phi, \sin\theta\sin\phi, \cos\theta)$. When applied on the state (2), neglecting virtual transitions and passing to the continuous limit, it yields $\hat{E}_S|\Psi\rangle = \mathcal{E}_S|g_1\ldots g_N\rangle$, where

$$\mathcal{E}_S(r,\theta,\phi,t) = \frac{dk_0^2}{4\pi\epsilon_0 r}e^{ik_0(r-ct)}\int \mathrm{d}\mathbf{r}' n(\mathbf{r}')\beta(\mathbf{r}',t)e^{-i\mathbf{k}\cdot\mathbf{r}'}. \tag{22}$$

Using the stationary solution (14) for a spherically symmetric distribution and using the integral

$$\int_0^\pi \mathrm{d}\theta' \sin\theta' P_n(\cos\theta')J_0(k_0 r'\sin\theta\sin\theta')e^{-ik_0 r'\cos\theta\cos\theta'} = 2i^{-n}j_n(k_0 r')P_n(\cos\theta) \tag{23}$$

we obtain

$$\mathcal{E}_S(r,\theta) = \left(\frac{E_0}{4\pi k_0 r}\right)e^{ik_0(r-ct)}\sum_{n=0}^{\infty}\frac{(2n+1)\lambda_n}{2\delta + i(1+\lambda_n)}P_n(\cos\theta), \tag{24}$$

where we used the relation $\Gamma = d^2k_0^3/(2\pi\hbar\epsilon_0)$. In the forward direction ($\theta = 0$) the scattered field is proportional to the 'phased' radiation amplitude (19). The expression (24) provides the angular distribution of the scattered radiation. We can also calculate the scattered intensity as

$$I_S(r,\theta,\phi) = c\epsilon_0\langle \hat{E}^\dagger\hat{E}\rangle = c\epsilon_0\left(\frac{dk_0^2}{4\pi\epsilon_0 r}\right)^2\left[\sum_{j=1}^{N}|\beta_j|^2 + \sum_{j\neq m}\beta_m^*\beta_j e^{-i\mathbf{k}\cdot(\mathbf{r}_j-\mathbf{r}_m)}\right] \tag{25}$$

Passing to the continuous limit and using Eqs.(20), (22) and (24), we obtain:

$$I_S(r,\theta) = \frac{I_0}{(4\pi k_0 r)^2}\left[\sum_{n=0}^{\infty}\frac{(2n+1)\lambda_n}{4\delta^2+(1+\lambda_n)^2} + \left|\sum_{n=0}^{\infty}\frac{(2n+1)\lambda_n}{2\delta+i(1+\lambda_n)}P_n(\cos\theta)\right|^2\right] \tag{26}$$

where $I_0 = c\epsilon_0 E_0^2$. The scattered intensity is the sum of the incoherent contribution, proportional to N (since $\lambda_n \propto N$, see Eq.(10)) and isotropic, and the superradiant contribution, proportional to N^2 and directed (for extended clouds) mainly in the forward direction. Integrating over the solid angle, the total scattered power is

$$P_S = 2\pi r^2\int_0^{\pi} d\theta \sin\theta I_S(r,\theta) = \left(\frac{I_0}{4\pi k_0^2}\right)\sum_{n=0}^{\infty}\frac{(2n+1)\lambda_n(1+\lambda_n)}{4\delta^2+(1+\lambda_n)^2} \tag{27}$$

where we used the second for the identities (18).

C. Radiation pressure force

The force operators along $\mathbf{k}_0 = k_0\hat{\mathbf{e}}_z$ acting on the center of mass of the atomic cloud and due to the absorption and emission processes, in the Markov approximation, are respectively

$$\hat{F}_a = \frac{i}{2N}\hbar k_0\Omega_0\sum_{j=1}^{N}\left[\hat{\sigma}_j e^{i\Delta_0 t - i\mathbf{k}_0\cdot\mathbf{r}_j} - \text{h.c.}\right] \tag{28}$$

$$\hat{F}_e = -\frac{\hbar k_0\Gamma}{8\pi N}\int_0^{2\pi}\mathrm{d}\phi\int_0^{\pi}\mathrm{d}\theta\sin\theta\cos\theta\sum_{j,m=1}^{N}\left[e^{-i\mathbf{k}\cdot(\mathbf{r}_j-\mathbf{r}_m)}\hat{\sigma}_m^{\dagger}\hat{\sigma}_j + \text{h.c.}\right]. \tag{29}$$

Evaluating their expectation values on the state (2) (neglecting virtual photon contributions), the emission force in the discrete model is

$$\begin{aligned}\langle F_e\rangle &= -\frac{\hbar k_0\Gamma}{8\pi N}\int_0^{2\pi}\mathrm{d}\phi\int_0^{\pi}\mathrm{d}\theta\sin\theta\cos\theta\sum_{j,m=1}^{N}\left[\beta_j\beta_m^* e^{-i\mathbf{k}\cdot(\mathbf{r}_j-\mathbf{r}_m)} + \text{c.c.}\right]\\ &= i\frac{\hbar k_0\Gamma}{2N}\sum_{j,m=1}^{N}\frac{(z_j-z_m)}{|\mathbf{r}_j-\mathbf{r}_m|}j_1(k_0|\mathbf{r}_j-\mathbf{r}_m|)(\beta_j\beta_m^* - \text{c.c.}).\end{aligned} \tag{30}$$

where we used the identity (A1) and $j_1(z)$ is the first order spherical Bessel function. Then, passing to the continuous distribution limit, Eqs.(28) and (29) are approximated by

$$\langle\hat{F}_a\rangle = -\hbar k_0\Omega_0\mathrm{Im}\langle\beta e^{-i\mathbf{k}_0\cdot\mathbf{r}}\rangle \tag{31}$$

$$\langle\hat{F}_e\rangle = -\hbar k_0\frac{\Gamma}{8\pi N}\int_0^{2\pi}\mathrm{d}\phi\int_0^{\pi}\mathrm{d}\theta\sin\theta\cos\theta\int d\mathbf{r}n(r)\int\mathrm{d}\mathbf{r}'n(r')\left[\beta(\mathbf{r})\beta^*(\mathbf{r}')e^{-i\mathbf{k}\cdot(\mathbf{r}-\mathbf{r}')} + \text{c.c.}\right]. \tag{32}$$

The absorption stationary force is readily obtained from Eq.(19),

$$\langle\hat{F}_a\rangle = \hbar k_0\frac{\Omega_0^2}{\Gamma N}\sum_{n=0}^{\infty}\frac{(2n+1)\lambda_n(1+\lambda_n)}{4\delta^2+(1+\lambda_n)^2} \tag{33}$$

whereas a longer calculation, reported in Appendix A, yields the emission stationary force,

$$\langle F_e\rangle = -\hbar k_0\frac{2\Omega_0^2}{\Gamma N}\sum_{n=0}^{\infty}\frac{(n+1)\lambda_n\lambda_{n+1}[4\delta^2+(1+\lambda_n)(1+\lambda_{n+1})]}{[4\delta^2+(1+\lambda_n)^2][4\delta^2+(1+\lambda_{n+1})^2]}. \tag{34}$$

As expected, the absorption force pushes the atomic cloud in the direction of the driving field, whereas the emission force is oppositely directed and is proportional to N. Both forces depend on N also through the collective decay rate $\Gamma(1+\lambda_n)$. We observe that the absorption force (33) is linked to the scattered power (27) by the relation

$$N\langle\hat{F}_a\rangle = 4\pi\left(\frac{P_S}{c}\right), \tag{35}$$

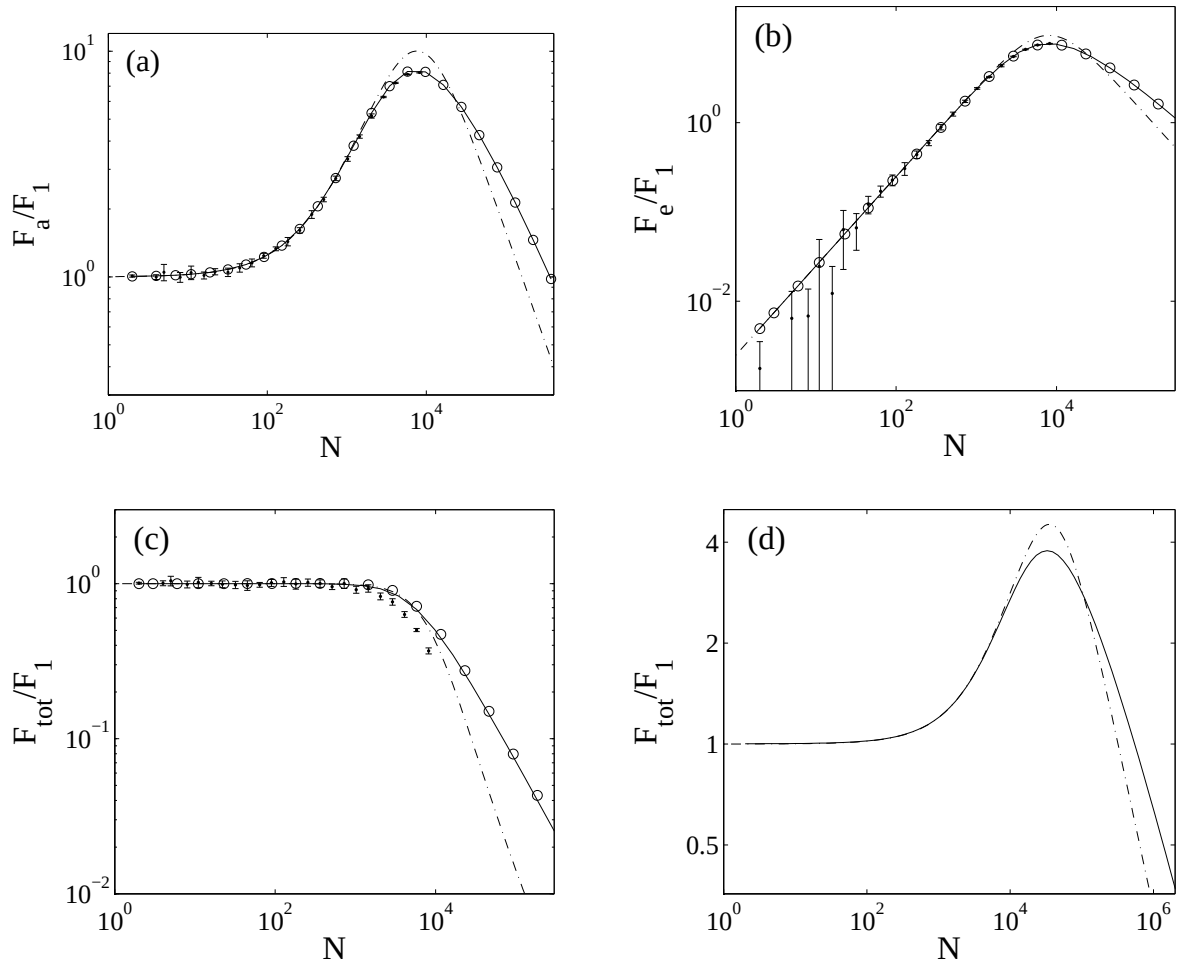

FIG. 1: (a) Absorption, (b) emission and (c) total forces vs N and for $\sigma = 8$ and $\delta = 10$. (d) Total force for $\sigma = 5$ and $\delta = 200$. Forces are relative to the single-atom force F_1. The plain curves refer to the series (33), (34) and their sum, the circles to the analytical expressions (44), (34) and their sum, the dots to N-body simulations (see Eq.4) and the dash-dotted lines to the STD state. The error bars correspond to the standard deviation of the observables over 8 realizations.

i.e. the absorption force is proportional to the scattered power per atom, P_S/N.

Fig.1 compares the (a) absorption, (b) emission and (c) total forces vs. N and for $\sigma = 8$ and $\delta = 10$, calculated using the series (33) and (34) (circles) and N-body simulations (see Eq.4) (dots). Forces are reported as a ratio between the cooperative force and the single-atom force, $F_1 = \hbar k_0 \Gamma \Omega_0^2/(4\Delta_0^2 + \Gamma^2)$. The error bars correspond to the standard deviation of the observables over 8 realizations. Fig.1d shows the total force vs. N for a different choice of parameters, $\sigma = 5$ and $\delta = 200$, for which the force exhibits a maximum as a function of N [7]. We observe a good agreement between the analytical solution (33) and the N-body simulations at large N, when effects due to the discreteness of the system become negligible.

We further comment that, although our expressions have been obtained in the continuous approximation limit, i.e. assuming a large number of atoms in a cubic optical wavelength volume, $N \gg \sigma^3$, our results remain valid also in the limit $N \to 0$ provided the sample size is much larger than an optical wavelength, $\sigma \gg 1$. In particular, for $N \to 0$ the standard radiation pressure force, F_1, is recovered. However, at low densities, fluctuations will strongly affect individual measurements of the radiation pressure force. In this regime, the expressions represent the average expectation values.

V. LARGE GAUSSIAN CLOUDS

Large clouds ($\sigma \gg 1$) behaves fundamentally differently from small clouds ($\sigma \lesssim 1$), as can be deduced from their spectrum. Let us for example consider the case of Gaussian clouds, with density $n(r) = (N/(2\pi)^{3/2}\sigma_R^3)\exp(-r^2/2\sigma_R^2)$. The spectrum then reads

$$\lambda_n = N\sqrt{\frac{2}{\pi}}\int_0^\infty \rho^2 e^{-\rho^2/2} j_n^2(\sigma\rho)\mathrm{d}\rho = N\sqrt{\frac{\pi}{2\sigma^2}}e^{-\sigma^2} I_{n+1/2}(\sigma^2), \tag{36}$$

where $\sigma = k_0\sigma_R$ is the scaled size of the cloud, and $I_n(x)$ the n-th modified Bessel function. Recently the spectrum λ_n for an uniform spherical cloud has been calculated by A.A. Svidzinsky et al. [4, 16], also for the exponential kernel of Eq.(3). However, a Gaussian distribution is certainly more realistic for experiments with cold dense atomic ensembles. Generally, the spectrum of small clouds ($\sigma \leq 1$) is composed of a few significant eigenmodes, whereas for σ large, all the eigenmodes for $n < \sigma$ are significant and the spectrum can be treated as a continuum. In particular, in the latter case the λ_n can be approximated, for $n < \sigma$, by $\lambda_n \sim (N/2\sigma^2)\exp[-(n+1/2)^2/2\sigma^2]$ (see e.g. [17]). Switching to a continuous treatment of the spectrum, we define $\eta = n + 1/2$ and get

$$\lambda_\eta = \frac{N}{2\sigma^2}e^{-\eta^2/(2\sigma^2)}. \tag{37}$$

$$\sum_{n=0}^{\infty}(2n+1) \to 2\int_0^\infty \eta\mathrm{d}\eta. \tag{38}$$

Remark that using these definitions, the completeness condition (15) is still preserved. The continuous spectrum limit allows for the evaluation of the sums in Eqs.(19) and (20) as continuous integrals

$$\langle\beta_s e^{-i\mathbf{k}_0\cdot\mathbf{r}}\rangle = \frac{2\Omega_0}{\Gamma N}\int_0^\infty \frac{\lambda_\eta\eta\mathrm{d}\eta}{2\delta + i(1+\lambda_\eta)} = \frac{\Omega_0}{\Gamma}\frac{6}{b_0}\int_0^{b_0/6}\frac{\mathrm{d}x}{2\delta + i(1+x)} \tag{39}$$

$$\langle|\beta_s|^2\rangle = \frac{2\Omega_0^2}{\Gamma^2 N}\int_0^\infty \frac{\lambda_\eta\eta\mathrm{d}\eta}{4\delta^2 + (1+\lambda_\eta)^2} = \left(\frac{\Omega_0}{\Gamma}\right)^2\frac{6}{b_0}\int_0^{b_0/6}\frac{\mathrm{d}x}{4\delta^2 + (1+x)^2} \tag{40}$$

where we have set $x = (b_0/6)\exp(-\eta^2/2\sigma^2)$, with $b_0 = 3N/\sigma^2$ the optical thickness. The above expressions integrate as

$$\langle\beta_s e^{-i\mathbf{k}_0\cdot\mathbf{r}}\rangle = \left(\frac{\Omega_0}{\Gamma}\right)\frac{3}{b_0}\left\{2\arctan\left[\frac{b_0}{3}\frac{\delta}{1+4\delta^2+b_0/6}\right] - i\ln\left[1+\frac{b_0}{3}\frac{1+b_0/12}{1+4\delta^2}\right]\right\} \tag{41}$$

$$\langle|\beta_s|^2\rangle = \left(\frac{\Omega_0}{\Gamma}\right)^2\frac{3}{\delta b_0}\arctan\left[\frac{\delta b_0/3}{1+4\delta^2+b_0/6}\right]. \tag{42}$$

These formulae highlight the prominent role of the parameters b_0 and δ in the high-density limit. In a similar way, we calculate the total scattered power as:

$$P_S = \frac{I_0 N}{4\pi k_0^2}\int_0^1 dx\frac{1+(b_0/6)x}{4\delta^2 + [1+(b_0/6)x]^2} = \frac{I_0\sigma_R^2}{4\pi}\ln\left[1+\frac{b_0}{3}\frac{1+b_0/12}{1+4\delta^2}\right] \tag{43}$$

As expected, for small optical thickness ($b_0 \ll 1$) the scattered power is incoherent, $P_S \approx [I_0 N/(4\pi k_0^2)]/(4\delta^2+1)$. However, for large optical thickness it shows a logarithmic dependence on N. The superradiant character of the radiation is visible only observing the scattered intensity in the forward direction (see the second term of Eq.(26)), but not in the total scattered power.

The absorption force is deduced from Eqs.(31) and (41) as

$$\langle\hat{F}_a\rangle = \hbar k_0\frac{3\Omega_0^2}{b_0\Gamma}\ln\left[1+\frac{b_0}{3}\frac{1+b_0/12}{1+4\delta^2}\right]. \tag{44}$$

The emission force can written, in the continuous spectrum approximation in the integral form

$$\langle\hat{F}_e\rangle = -\hbar k_0\frac{\Omega_0^2 b_0}{6\Gamma}e^{-1/(4\sigma^2)}\int_{1/\sigma}^\infty dy\frac{ye^{-y^2}\left\{4\delta^2+\left[1+(b_0/6)e^{-(y+1/2\sigma)^2/2}\right]\left[1+(b_0/6)e^{-(y-1/2\sigma)^2/2}\right]\right\}}{\left\{4\delta^2+\left[1+(b_0/6)e^{-(y+1/2\sigma)^2/2}\right]^2\right\}\left\{4\delta^2+\left[1+(b_0/6)e^{-(y-1/2\sigma)^2/2}\right]^2\right\}}, \tag{45}$$

where we have set $y = (\eta+1)/\sigma$. As can be observed in Fig.1, the continuous-spectrum approximation gives excellent results compared to the full series (33) and (34). In the limit $\sigma \to \infty$ and finite b_0, Eq.(45) would lead to

$$\langle \hat{F}_e \rangle \approx -\langle \hat{F}_a \rangle + \hbar k_0 \Gamma \langle |\beta_s|^2 \rangle, \tag{46}$$

which has a transparent interpretation: for a very large cloud, the atoms scatter radiation in the forward direction and the recoil received by the atoms upon emission cancels out with the recoil received by absorbing a photon from the driving field. The net force remaining after the substraction is the non collective contribution to the emission. The net force is equal to the photon momentum $\hbar k_0$ times the emission rate $\Gamma\langle|\beta_s|^2\rangle$. This emission rate depends indirectly on N and σ through the enhanced superradiant decay, $\Gamma(N/4\sigma^2)$, which decreases the emission rate when the optical thickness increases. A more accurate expression of the emission force valid for large but finite cloud size would require the exact evaluation of the integral in Eq.(45).

VI. SYMMETRIC TIMED DICKE STATE

A particular ansatz used by Scully and coworkers [4, 15, 16] is the symmetric timed Dicke (STD) state, given by

$$\beta(\mathbf{r}, t) = \beta_{TD}(t) e^{i\mathbf{k}_0 \cdot \mathbf{r}}. \tag{47}$$

After integration over space of Eq.(5), one obtains the following evolution equation

$$\frac{d\beta_{TD}(t)}{dt} = \left[i\Delta_0 - \frac{\Gamma}{2}(1 + N s_\infty) \right] \beta_{TD}(t) - i\frac{\Omega_0}{2}, \tag{48}$$

where s_∞ is the integrated structure factor of the cloud defined as

$$s_\infty = \frac{1}{N^2} \int n(\mathbf{r}) \mathrm{d}\mathbf{r} \int \mathrm{d}\mathbf{r}' n(\mathbf{r}') \frac{\sin(k_0|\mathbf{r}-\mathbf{r}'|)}{k_0|\mathbf{r}-\mathbf{r}'|} e^{-i\mathbf{k}_0 \cdot (\mathbf{r}-\mathbf{r}')} = \frac{1}{4\pi} \int_0^{2\pi} \mathrm{d}\phi \int_0^{\pi} \mathrm{d}\theta \sin\theta |\langle e^{i(\mathbf{k}_0 - \mathbf{k}) \cdot \mathbf{r}} \rangle|^2. \tag{49}$$

This ansatz is of particular interest since it allows to evidence e.g. the superradiant nature of the decay of such state when the pump is turned off [19]. As for its steady-state, it reads [5, 6]

$$\beta_{TD} = \frac{\Omega_0}{\Gamma} \frac{1}{2\delta + i(1 + N s_\infty)}, \tag{50}$$

and for a large cloud with Gaussian distribution, since $s_\infty \approx 1/4\sigma^2$, we get

$$\beta_{TD} = \frac{\Omega_0}{\Gamma} \frac{1}{2\delta + i(1 + b_0/12)}. \tag{51}$$

Thus, the STD solution (51) approximates the exact result (42) only for $b_0 \ll 12$,

$$|\beta_{TD}|^2 \approx \left(\frac{\Omega_0}{\Gamma} \right)^2 \frac{1}{4\delta^2 + (1 + b_0/6)}. \tag{52}$$

Fig.2 shows the average excitation probability $\langle|\beta_s|^2\rangle$ (left) and its variance, $\sigma_\beta^2 = \langle|\beta_s|^2\rangle - |\langle\beta_s e^{-ik_0\cdot\mathbf{r}}\rangle|^2$ vs. N for $\sigma = 10$ and $\delta = 10$. The plain curves refer to the analytical expressions (41) and (42), the circles to series expressions (19) and (20), the dots to N-body simulations (see Eq.4) and the dash-dotted lines to the STD state (47). The error bars correspond to the standard deviation of the observables over different realizations. Note that for the STD state, $\sigma_\beta = 0$; for too small N, the approximations (41) and (42) provide inconsistent results, that is negative σ_β. We observe excellent agreement between the series and the analytical solutions, and a consistent reduction of the excitation probability decrease vs N with respect to the TDS prediction (dashed line in fig.2, left). Also the fluctuations obtained from the N-body simulations converge for large values of N toward the results obtained in the continuous density approximation (fig.2, left), showing the presence of a shot-noise contribution for small N.

The radiation force for the STD ansatz (47) is [5–7]

$$\langle \hat{F} \rangle = \langle \hat{F}_a \rangle + \langle \hat{F}_e \rangle = \hbar k_0 \left[-\Omega_0 \mathrm{Im}(\beta_{TD}) - \Gamma |\beta_{TD}|^2 N f_\infty \right] \tag{53}$$

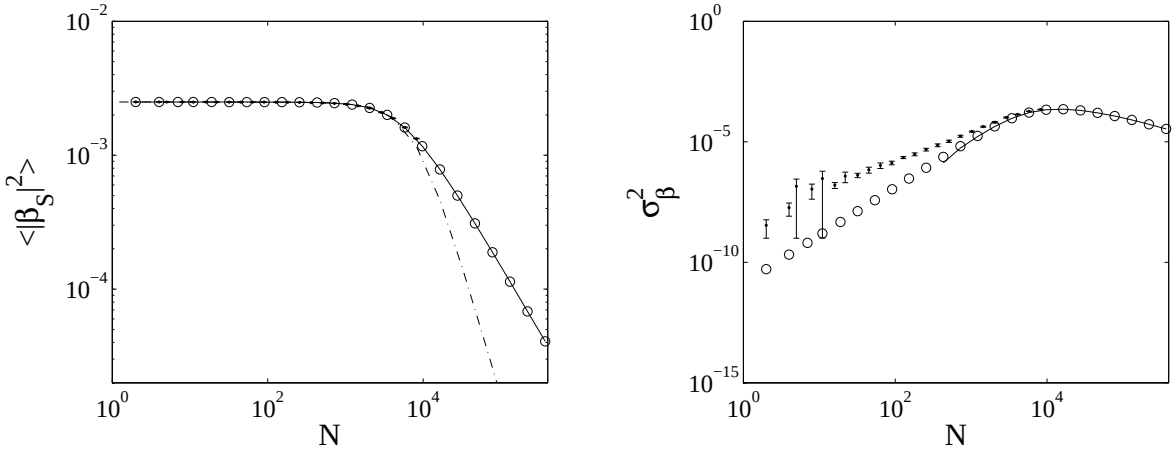

FIG. 2: Average excitation probability $\langle|\beta_s|^2\rangle$ (left) and variance $\sigma_\beta^2 = \langle|\beta_s|^2\rangle - |\langle\beta_s e^{-ik_0\cdot\mathbf{r}}\rangle|^2$ (right) vs N. The plain curves refer to the analytical expressions (41) and (42), the circles to series expressions (19) and (20), the dots to N-body simulations (see Eq.4) and the dash-dotted lines to the STD state. The error bars correspond to the standard deviation of the observables over 8 realizations. Note that for the STD state, $\sigma_\beta = 0$; for too small N, the approximations (41) and (42) provide inconsistent results, that is negative σ_β. Simulations realized for $\sigma = 10$ and $\delta = 10$.

where

$$f_\infty = \frac{1}{4\pi}\int_0^{2\pi} \mathrm{d}\phi \int_0^{\pi} \mathrm{d}\theta \sin\theta\cos\theta |\langle e^{i(\mathbf{k}_0-\mathbf{k})\cdot\mathbf{r}}\rangle|^2. \tag{54}$$

Since for a spherically Gaussian distribution $N(s_\infty - f_\infty) \approx N/(8\sigma^4) = b_0/(24\sigma^2)$, from Eq.(50) the stationary radiation force is [5–7]

$$\langle\hat{F}\rangle = \hbar k_0\Gamma\left(\frac{\Omega_0}{\Gamma}\right)^2 \frac{1+N(s_\infty - f_\infty)}{4\delta^2 + (1+Ns_\infty)^2} \tag{55}$$

$$\approx \hbar k_0\Gamma\left(\frac{\Omega_0}{\Gamma}\right)^2 \frac{1+b_0/24\sigma^2}{4\delta^2 + (1+b_0/12)^2}. \tag{56}$$

As can be observed in Fig.1, the STD state yields a good agreement with the full-spectrum approach and the N-body simulations only for small values of the optical thickness.

Finally, for that state (47) the scattered radiation electric field, Eq.(21), and intensity, (25), become

$$\mathcal{E}_S(r,\theta,\phi,t) = \frac{dk_0^2}{4\pi\epsilon_0 r} e^{ik_0(r-ct)}\beta_{TD}(t)\langle e^{i(\mathbf{k}_0-\mathbf{k})\cdot\mathbf{r}}\rangle \tag{57}$$

and

$$I_S(r,\theta,\phi) = c\epsilon_0\left(\frac{dk_0^2}{4\pi\epsilon_0 r}\right)^2 |\beta_{TD}|^2\left[N + N^2|\langle e^{i(\mathbf{k}_0-\mathbf{k})\cdot\mathbf{r}}\rangle|^2\right]. \tag{58}$$

In particular, for a Gaussian distribution, $\langle\exp[i(\mathbf{k}_0-\mathbf{k})\cdot\mathbf{r}]\rangle = \exp[-\sigma^2(1-\cos\theta)/2]$.

Fig.3 shows the phase of the excitation amplitude β_s (left) and the excitation probability, $|\beta_s|^2$, (center) in the (x,z) plane ($y=0$), calculated from the exact solution (14), for $N = 10^4$, $\sigma = 10$ and $\delta = 10$. Fig.3 (right) shows the contribution to the electric field radiation in the same plane, weighted by the local atomic density. The simplification of the STD, as compared to the exact solution (14), resides in the assumption that all atoms are equally excited and oscillate in phase. According to the exact calculation, the atomic dipoles appear to be in phase only in the core of the cloud (see Fig.3, left), but this phase profile has strong distortion away from it. This phenomenon is all the more important as the atoms are much more excited in the peripheral region than in the core (see Fig.3, center). In particular, even when this excitation probability is weighted by the particle density, two areas at the cloud entrance and exit contribute significantly to the radiation electric field (24) (see peaked structures in Fig.3, right). For a timed Dicke state, both the phase profile and average excitation remain flat throughout the cloud. From a macroscopic

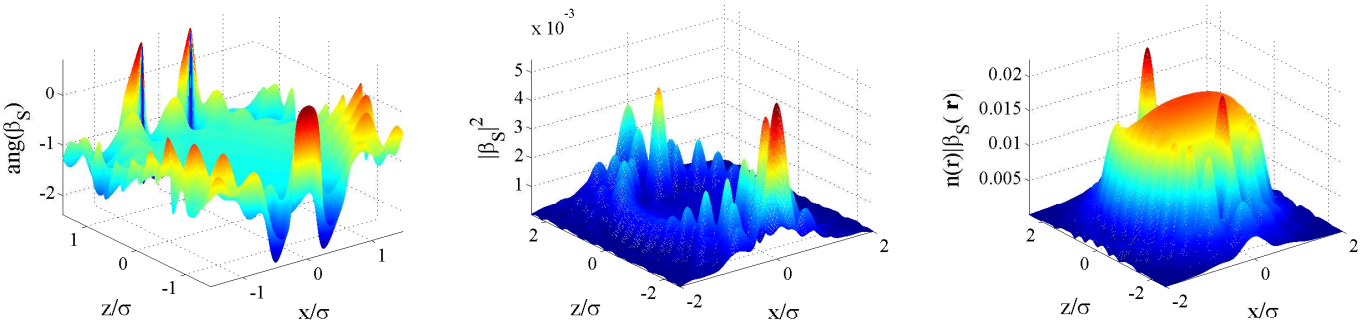

FIG. 3: Phase of the atomic radiation $ang(\beta_s)$ (left), Excitation probability $|\beta_s|^2$ of the atoms in the (x, z) plane $(y = 0)$ (center) and contribution to the radiation of the electric field in the same plane, which corresponds to the level of excitation of the atoms weighted by their local density (right). Simulations realized using the analytic expressions (14), for $N = 10^4$, $\sigma = 10$ and $\delta = 10$.

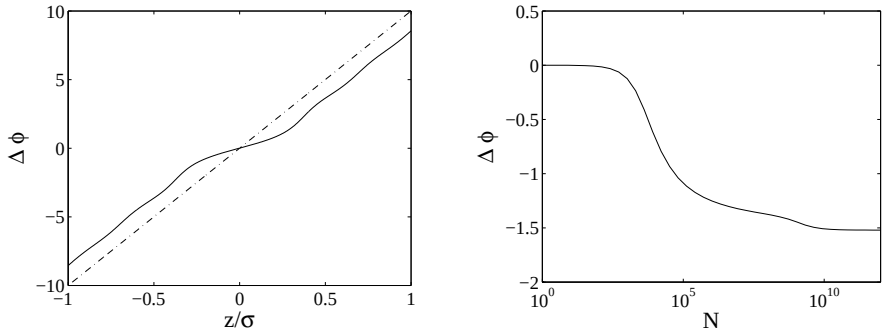

FIG. 4: Left: Phase shift along the optical axis for the exact solution (14) (plain line) and a STD state (47) (dash-dotted line). Right: Phase shift of the pump beam after transmission through the cloud as a function of N evaluated along the axis , $x = y = 0$, at $k_0 z = 20\sigma$, for $N = 10^4$, $\sigma = 10$ and $\delta = 10$.

point of view, the STD state neglects phase shifts imprinted into the pump beam by the cloud's reflective index. This can be seen in Fig. 4(a), which compares the phase of the STD state, $\beta_{TD} \exp(i\mathbf{k}_0 \cdot \mathbf{r})$, (linear curve, no phase shift) and $\beta_s(\mathbf{r})$ (additional phase-shift) along the optical axis across the cloud. Fig. 4(b) shows the pump beam phase shift after transmission through the atomic cloud as a function of atom number. This phase shift is at the origin of the deviation between the radiation pressure forces calculated for the STD state and the exact solution. The pump beam phase shift leads to a reduction of the absorption and the emission forces. This can be understood as destructive interference of forward radiation emitted from different atoms, located at the same plane $z = z_0$ but different x or y.

As for the emitted wave, it is concentrated in the forward direction (see Fig.5, left), and there is no backscattering (not shown here). The wavefront phase does not exhibit significant distortion in the central region of the radiated beam (see Fig.5, right).

VII. CONCLUSIONS

We analyzed the collective scattering problem from a dense and large atomic cloud in terms of the eigenvalues of the interaction operator, for gaussian density profiles. One crucial approximation is that the system is sufficiently diluted and the size large enough to neglect short-range effects due to dipole-dipole interactions, even if the atoms are eventually treated as a continuous density.

Our approach consisted in expanding the solution on spherical harmonics which form a complete orthogonal basis of the hermitian interaction matrix. Furthermore, the continuous spectrum approximation allows to transform infinite series into solvable integrals, and eventually to derive analytical expressions for the most relevant observables, such as the scattered intensity and radiation pressure force. These analytical expressions show good agreement with the numerical solution of the N-body problem, and highlight the dependence on the accessible experimental parameters such as optical thickness, atomic cloud size and laser frequency.

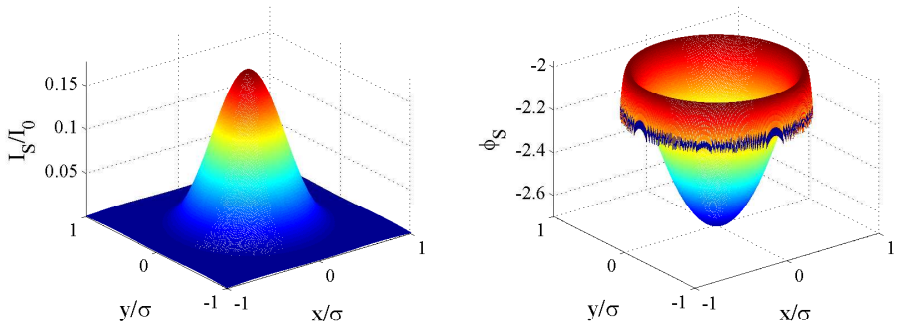

FIG. 5: Transverse intensity profile (left) of the wave emitted by the cloud, at $z = 3\sigma$ and its wavefront (right). Simulations realized using the analytic expression (24), for $N = 10^4$, $\sigma = 10$ and $\delta = 10$.

The analytical solution appears particularly useful for studying the thermodynamics limit when $N \to \infty$ and $V \to \infty$ with N/V fixed, until collisions or non resonant interactions come into play. The thermodynamic limit is hardly accessible to N-body simulations, since the latter are highly CPU consuming.

In contrast, the eigenvalue approach opens the possibility to study the fascinating link between microscopic and macroscopic domains of light scattering, and in particular between single-atom scattering and Mie scattering for extended continuous samples [3]. For large optical thickness, the refraction index of the cloud acts back on the driving field and shifts its phase.

For these reasons, the solution for large optical thickness shows appreciable deviations from that obtained assuming a symmetric timed Dicke state for the atomic sample, since the latter corresponds to a completely degenerate eigenvalue spectrum. On the contrary, our spectrum is approximately Gaussian with a size equal to $\sigma = k_0\sigma_R$. The exact solution (14) takes into account the induced phase shift and reduces to the symmetric timed Dicke state in the limit of relatively small optical thickness. An important further development of the present study should be to understand how the dipole-dipole interactions contribute to the observed cooperative effects, completing in this way the cooperative scattering description for highly compressed and dense atomic clouds.

VIII. ACKNOWLEDGEMENTS

We acknowledge fruitful discussions with R. Kaiser and T. Bienaimé.

Appendix A: Derivation of Eq.(34)

The angular integral in Eq.(32) is

$$\int_0^{2\pi} \mathrm{d}\phi \int_0^{\pi} \mathrm{d}\theta \sin\theta \cos\theta e^{-i\mathbf{k}\cdot(\mathbf{r}-\mathbf{r}')} = 4\pi i \frac{z-z'}{|\mathbf{r}-\mathbf{r}'|} j_1(k_0|\mathbf{r}-\mathbf{r}'|). \tag{A1}$$

Since

$$\frac{\partial}{\partial z} j_0(k_0|\mathbf{r}-\mathbf{r}'|) = -k_0 \frac{(z-z')}{|\mathbf{r}-\mathbf{r}'|} j_1(k_0|\mathbf{r}-\mathbf{r}'|),$$

where $j_0(x) = \sin(x)/x$, Eq.(32) can be written as

$$\langle \hat{F}_e \rangle = -i\frac{\hbar k_0 \Gamma}{2N} \int \mathrm{d}\mathbf{r} n(r) \left\{ \beta(\mathbf{r}) \frac{\partial}{\partial(k_0 z)} \int \mathrm{d}\mathbf{r}' n(r') j_0(k_0|\mathbf{r}-\mathbf{r}'|) \beta^*(\mathbf{r}') - \text{c.c.} \right\}. \tag{A2}$$

Using the expansions (6) and (8) and Eqs.(7) and (10), we obtain

$$\int d\mathbf{r}' n(\mathbf{r}') j_0(k_0|\mathbf{r}-\mathbf{r}'|) \beta^*(\mathbf{r}') = \sum_{n=0}^{\infty} \sum_{m=-n}^{n} \alpha_{nm}^* \lambda_n j_n(k_0 r) Y_{nm}^*(\theta, \phi). \tag{A3}$$

In spherical coordinates

$$\frac{\partial}{\partial z} = \cos\theta \frac{\partial}{\partial r} + \frac{\sin^2\theta}{r}\frac{\partial}{\partial \cos\theta}$$

and

$$\langle \hat{F}_e \rangle = -i\frac{\hbar k_0 \Gamma}{2N} \int \mathrm{d}\mathbf{r} n(r) \left\{ \beta(\mathbf{r}) \sum_{n=0}^{\infty} \sum_{m=-n}^{n} \alpha_{nm}^* \lambda_n \left(\cos\theta \frac{\partial}{\partial(k_0 r)} + \frac{\sin^2\theta}{k_0 r}\frac{\partial}{\partial\cos\theta} \right) j_n(k_0 r) Y_{nm}^*(\theta,\phi) - \text{c.c.} \right\} \quad \text{(A4)}$$

Still using Eq.(8),

$$\begin{aligned} \langle \hat{F}_e \rangle &= -\frac{\hbar k_0 \Gamma}{2N} \sum_{p=0}^{\infty} \sum_{q=-p}^{p} \sum_{n=0}^{\infty} \sum_{m=-n}^{n} \lambda_n \int_0^{\infty} \mathrm{d}r r^2 n(r) j_p(k_0 r) \int_0^{2\pi} \mathrm{d}\phi \int_0^{\pi} \mathrm{d}\theta \sin\theta \times \\ &\times \left\{ \frac{\partial j_n(k_0 r)}{\partial(k_0 r)} \cos\theta \, Y_{pq}(\theta,\phi) Y_{nm}^*(\theta,\phi) + \frac{j_n(k_0 r)}{k_0 r} \sin^2\theta \, Y_{pq}(\theta,\phi) \frac{\partial Y_{nm}^*(\theta,\phi)}{\partial(\cos\theta)} \right\} i \left(\alpha_{pq} \alpha_{nm}^* - \text{c.c.} \right). \end{aligned} \quad \text{(A5)}$$

Assuming as before

$$\alpha_{nm} = \alpha_n \delta_{m,0}$$

and since

$$Y_{n0}(\theta,\phi) = \sqrt{\frac{2n+1}{4\pi}} P_n(\cos\theta),$$

Eq.(A5) becomes

$$\begin{aligned} \langle \hat{F}_e \rangle &= -\frac{\hbar k_0 \Gamma}{4N} \sum_{p=0}^{\infty} \sum_{n=0}^{\infty} \lambda_n \sqrt{(2n+1)(2p+1)} \int_0^{\infty} \mathrm{d}r r^2 n(r) j_p(k_0 r) \int_0^{\pi} d\theta \sin\theta \times \\ &\times \left\{ \frac{\partial j_n(k_0 r)}{\partial(k_0 r)} \cos\theta \, P_p(\cos\theta) P_n(\cos\theta) + \frac{j_n(k_0 r)}{k_0 r} \sin^2\theta \, P_p(\cos\theta) \frac{\partial P_n(\cos\theta)}{\partial(\cos\theta)} \right\} i \left(\alpha_p \alpha_n^* - \text{c.c.} \right). \end{aligned} \quad \text{(A6)}$$

Since

$$\int_0^{\pi} d\theta \sin\theta \cos\theta \, P_p(\cos\theta) P_n(\cos\theta) = \int_{-1}^{1} \mathrm{d}x x P_n(x) P_p(x)$$

and

$$\int_0^{\pi} \mathrm{d}\theta \sin^3\theta P_p(\cos\theta) \frac{\partial P_n(\cos\theta)}{\partial(\cos\theta)} = \int_{-1}^{1} \mathrm{d}x (1-x^2) P_p(x) \frac{\mathrm{d}}{\mathrm{d}x} P_n(x),$$

using the identities

$$(2p+1) x P_p(x) = (p+1) P_{p+1}(x) + p P_{p-1}(x),$$

$$(x^2-1)\frac{dP_n(x)}{dx} = n\left[x P_n(x) - P_{n-1}(x) \right]$$

and

$$\int_{-1}^{1} \mathrm{d}x P_n(x) P_p(x) = \frac{2}{2n+1} \delta_{n,p},$$

we obtain

$$\int_{-1}^{1} \mathrm{d}x x P_n(x) P_p(x) = \frac{2}{(2p+1)(2n+1)} \left\{ (p+1)\delta_{n,p+1} + p\,\delta_{p,n+1} \right\}$$

and

$$\int_{-1}^{1} \mathrm{d}x(x^2-1)P_p(x)\frac{\mathrm{d}}{\mathrm{d}x}P_n(x) = \frac{2n}{(2n+1)(2p+1)}\left\{p\,\delta_{p,n+1} - (n+1)\delta_{n,p+1}\right\}.$$

By substituting these expressions in Eq.(A6) we obtain

$$\begin{aligned}\langle \hat{F}_e \rangle &= -\frac{\hbar k_0 \Gamma}{2N}\sum_{p=0}^{\infty}\sum_{n=0}^{\infty} i(\alpha_p\alpha_n^* - \text{c.c.})\frac{\lambda_n}{\sqrt{(2n+1)(2p+1)}}\int_0^{\infty}\mathrm{d}r r^2 n(r) j_p(k_0 r)\times \\ &\times \left\{(p+1)\left[\frac{\partial j_{p+1}(k_0 r)}{\partial(k_0 r)} + (p+2)\frac{j_{p+1}(k_0 r)}{k_0 r}\right]\delta_{n,p+1} + p\left[\frac{\partial j_n(k_0 r)}{\partial(k_0 r)} - n\frac{j_n(k_0 r)}{k_0 r}\right]\delta_{p,n+1}\right\}. \qquad \text{(A7)}\end{aligned}$$

Since

$$\frac{dj_{n+1}(z)}{dz} = j_n(z) - \frac{n+2}{z}j_{n+1}(z)$$

and

$$\frac{dj_n(z)}{dz} = -j_{n+1}(z) + \frac{n}{z}j_n(z),$$

using the definition (10),

$$\langle \hat{F}_e \rangle = -\frac{\hbar k_0 \Gamma}{8\pi N}\sum_{p=0}^{\infty}\sum_{n=0}^{\infty} i(\alpha_p\alpha_n^* - \text{c.c.})\frac{\lambda_n\lambda_p}{\sqrt{(2n+1)(2p+1)}}\left\{(p+1)\delta_{n,p+1} - p\delta_{p,n+1}\right\}. \qquad \text{(A8)}$$

Eliminating one of the two sums, we obtain:

$$\langle \hat{F}_e \rangle = -\frac{\hbar k_0 \Gamma}{4\pi N}\sum_{n=0}^{\infty}\frac{(n+1)\lambda_n\lambda_{n+1}}{\sqrt{(2n+1)(2n+3)}} i(\alpha_n\alpha_{n+1}^* - \text{c.c.}). \qquad \text{(A9)}$$

In the stationary case,

$$\alpha_n = \frac{\Omega_0}{\Gamma}\frac{i^n\sqrt{4\pi(2n+1)}}{2\delta + i(1+\lambda_n)}$$

and the stationary force is

$$\langle F_e \rangle = -\hbar k_0 \frac{2\Omega_0^2}{\Gamma N}\sum_{n=0}^{\infty}\frac{(n+1)\lambda_n\lambda_{n+1}[4\delta^2 + (1+\lambda_n)(1+\lambda_{n+1})]}{[4\delta^2 + (1+\lambda_n)^2][4\delta^2 + (1+\lambda_{n+1})^2]}. \qquad \text{(A10)}$$

[1] H. C. van de Hulst, Light Scattering by Small Particles (Dover Publications, New York, 1981).
[2] R.H. Dicke, Phys. Rev. **93**,99 (1954).
[3] S. Prasad, R.J. Glauber, Phys. Rev. A **82**, 063805 (2010).
[4] A. A. Svidzinsky, J.-T. Chang, and M. O. Scully, Phys. Rev. A **81**, 053821 (2010).
[5] Ph.W. Courteille, S. Bux, E. Lucioni, K. Lauber, T. Bienaimé, R. Kaiser, N. Piovella, Eur. J. Phys. D **58**, 69 (2010).
[6] T. Bienaimé, S. Bux, E. Lucioni, Ph. W. Courteille, N. Piovella, and R. Kaiser, Phys. Rev. Lett. **104**, 183602 (2010).
[7] H. Bender, C. Stehle, S. Slama, R. Kaiser, N. Piovella, C. Zimmermann, and Ph. W. Courteille, Phys. Rev. A **82**, 011404 (2010).
[8] R. Bonifacio, L. De Salvo, L. M. Narducci, and E. J. DAngelo, Phys. Rev. A 50, 1716 (1994).
[9] S. Slama, G. Krenz, S. Bux, C. Zimmermann, and P. W. Courteille, Phys. Rev. A 75, 063620 (2007).
[10] S. Inouye, A. P. Chikkatur, D. M. Stamper-Kurn, J. Stenger, D. E. Pritchard, and W. Ketterle, Science 285, 571 (1999).
[11] L. Fallani, C. Fort, N. Piovella, M. M. Cola, F. S. Cataliotti, M. Inguscio, and R. Bonifacio, Phys. Rev. A 71, 033612 (2005).
[12] M. G. Moore, O. Zobay, and P. Meystre, Phys. Rev. A 60, 1491 (1999).
[13] S. Bux et al., arXiv1101.2391

[14] R. Friedberg, S.R, Hartman, and J.T. Manassah, Phys. Rep. **7** 101 (1973).
[15] M.O. Scully, E. Fry, C.H.R. Ooi, and K. Wodkiewicz, Phys. Rev. Lett. **96**, 010501 (2006).
[16] A. A. Svidzinsky, J.-T. Chang, and M. O. Scully, Phys. Rev. Lett. **100**, 160504 (2008).
[17] M. Abramowitz and I.A. Stegun, *Handbook of Mathematical Functions*, p. 377.
[18] I. S. Gradshteyn and I. M. Ryzhik *Table of Integrals, Series, and Products*, Alan Jeffrey and Daniel Zwillinger (eds.), Seventh edition (Feb 2007), p. 885.
[19] M. O. Scully and A. A. Svidzinsky, *Phys. Lett. A* **373** (14) 1283 (2009)
[20] M. O. Scully and A. A. Svidzinsky, *Science* **4 328** 1239 (2010)
[21] R. Röhlsberger, K. Schlage, B. Sahoo, S. Couet and R. Rüffer, *Science* **328**, 1239 (2010).
[22] A. A. Svidzinsky, M. O. Scully, *Opt. Comm.* **282** (14) 2894 (2009)